# Wind-Related Modification of Some Small Impact Craters on Mars

Ruslan O. Kuzmin

*Vernadsky Institute, Russian Academy of Sciences, Kosygin St 19, Moscow 117975 GSP-1, Russia*
E-mail: Greeley@asu.edu

Ronald Greeley

*Department of Geology, Arizona State University, Box 871404, Tempe, Arizona 85287-1404*

Scot C. R. Rafkin

*Department of Meteorology, San Jose State University, San Jose, California 95192-0104*

and

Robert Haberle

*NASA-Ames Research Center, Moffett Field, California 94035-1000*

Inferred wind-related modifications of impact craters are observed in the vicinity of the Mars Pathfinder (MPF) site and in other regions of Mars. Mars Obiter Camera (MOC) images show three types of inferred wind-modified morphologies for craters 0.3–1 km in diameter. Such modifications could be related to seasonal variations of the strongest winds and a possible paleowind regime. Geomorphic mapping of Big Crater at the MPF shows evidence of former aeolian modification of the crater rim and interiors similar to smaller craters in the area. The morphologic patterns are in good agreement with the results from the Mars Regional Atmospheric Modeling Simulation (MRAMS) of topographically forced wind circulation and atmosphere-surface interactions generated by flow over small craters. Simulations show that the maximum surface stress is on the downwind crater rim, consistent with inferred wind modification of the crater rim seen in MOC images. The trend of the inferred paleowind regime at the MPF site cannot be explained by a change in the global atmospheric circulation resulting from changes in Mars' obliquity. We suggest that this wind regime could be associated with a regional meteorological pattern that is not modeled by global scale circulation. An alternative explanation is that Mars' spin axis was in a different geographic position than it is at present. © 2001 Academic Press

## 1. INTRODUCTION

High resolution Mars Obiter Camera (MOC) images of the Mars Pathfinder (MPF) site obtained from 1997 to 1999 show that in the postflood period the area has been subjected primarily to aeolian processes and associated resurfacing (Smith *et al.* 1998; Greeley *et al.* 1999). Images from the Mars Pathfinder lander (IMP) and MOC show a variety features attributed to wind erosion and deposition, including wind tails, duneforms, bright transverse dunes, bright wind streaks, and intracrater deposits. The orientation of these aeolian features is consistent with the direction of current strong winds in the area (Greeley *et al.* 1999, 2000).

Evidence for the modification of the rims of some small impact craters by wind was suggested by Kuzmin and Greeley (1999, 2000) and Greeley *et al.* (2000). The paper describes small craters inferred to have been modified by winds primarily in the area around the MPF site. Most craters are secondaries 60–300 m in diameter which formed in the postflood period. Their west-northwest rims have been degraded or removed, which was interpreted as evidence for paleowinds blowing from the southeast. This interpretation was based on two considerations. First, the modified parts of the rim are positioned 90° from the current wind regime (defined by the GCM and other aeolian features, such as wind streaks seen from orbit). Second, the azimuths of the modified crater rim sectors are very similar to those of the ventifacts at the MPF site and for the dunes on the floor of Big Crater. However, the interpretation of the degraded crater rims and the bright ridges as duneforms might be influenced by illumination conditions and the resolution of the MOC images; moreover, the bright ridges could be fluvial features related to Tiu Valles (Golombek and Bridges, 2000) which are covered with windblown material (Ward *et al.* 1999). To address these possibilities, we analyzed the features using MOC stereo-images and images of the MPF area taken under different
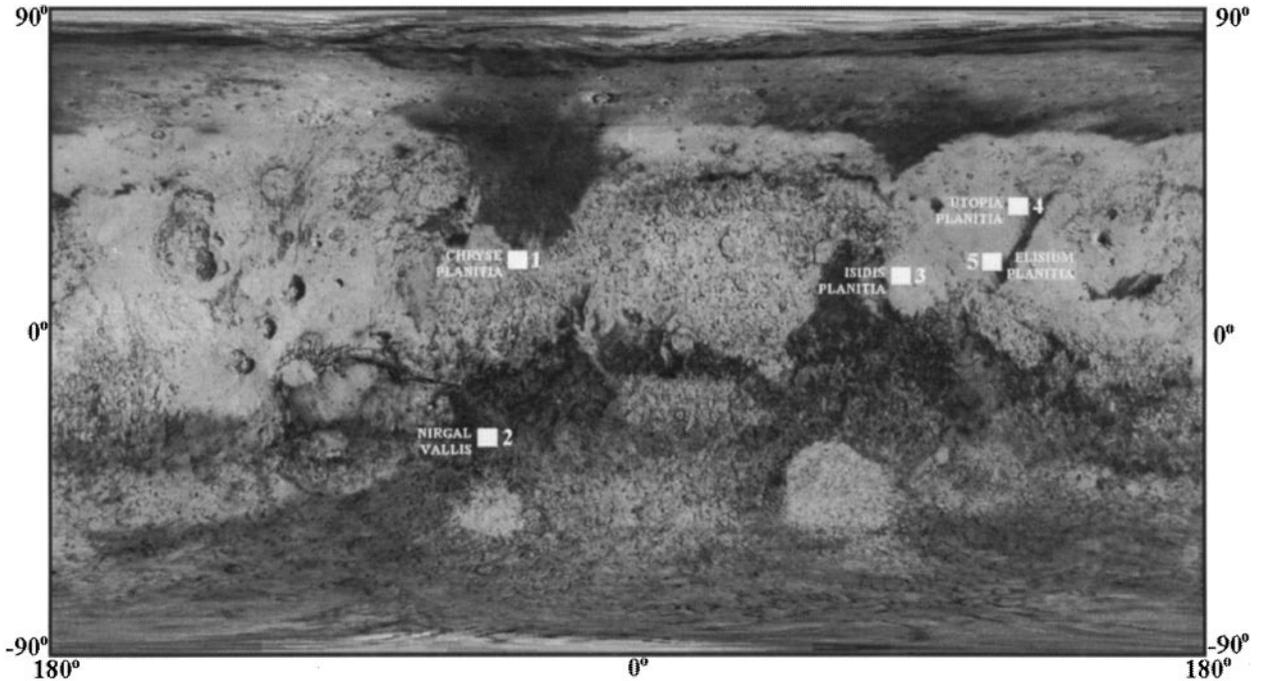
**FIG. 1.** Map of Mars showing the locations where MOC images were analyzed: (1) MPF site area in Chryse Planitia; (2) Nirgal Vallis region; (3) Isidis, (4) Utopia Planitia and (5) Elysium Planitia.

illumination and at higher resolution than those used in the previous studies. To determine if there are similar wind modified craters elsewhere, we also analyzed the MOC images of other regions, shown on Fig. 1. Finally, results from morphologic analysis and mapping of Big Crater were combined with predictions from a mesoscale model of atmospheric circulation-generated flow over a stylized crater at the MPF site.

## 2. OBSERVATIONS

### 2.1. Wind-Related Modification of Impact Craters in the MPF Area

Our study is based on the analysis of MOC images 21803, 23703, 25603, and M11-2414, which range in resolution from 2.4 to 7.3 m/pixel. In the study area, there are no pristine impact craters, nor distinctive ejecta blankets around the small craters. Our study focused on the morphology of the crater interiors and rims and an assessment of their modification by aeolian processes. The analyzed craters range in diameter from 0.060 to 1.3 km. Eighty percent of 105 craters analyzed in the MPF area (4.75 km by 6.04 km) have their west-northwest rims degraded by erosion or by mantling with aeolian deposits. The azimuths for the degraded part of the rims (measured from the crater center through the middle of degraded part of the rim) range from $253°$ to $317°$, with an average of $294°$ (Fig. 2). We found that the older craters generally have the most degraded of the rim segments, while intermediate-age craters have less degraded rim segments, and the youngest craters have completely preserved

rims (Fig. 3). Because none of the current wind directions in the area are consistent with the azimuths of the crater rim modification, this result is interpreted as a morphologic indicator of a stronger wind regime in the past.

Aeolian features such as intra-crater aeolian deposits and the bright streaks are associated with younger craters, consistent
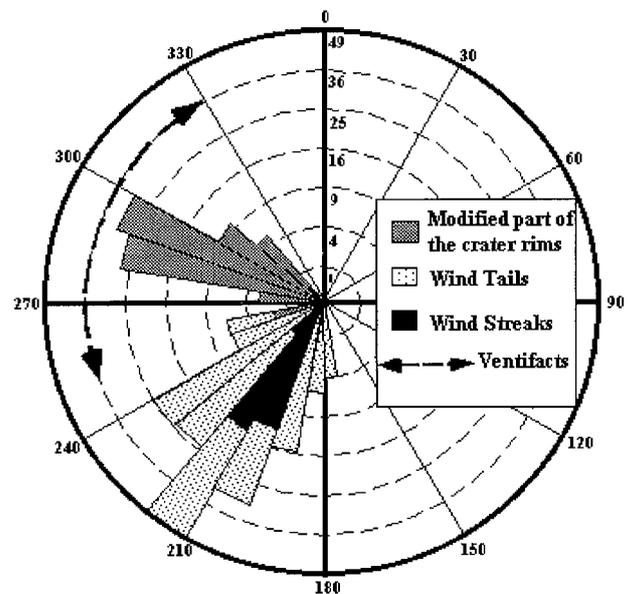


**FIG. 2.** Rose-diagram of the azimuth frequencies for the wind-modified rim segments of small impact craters.
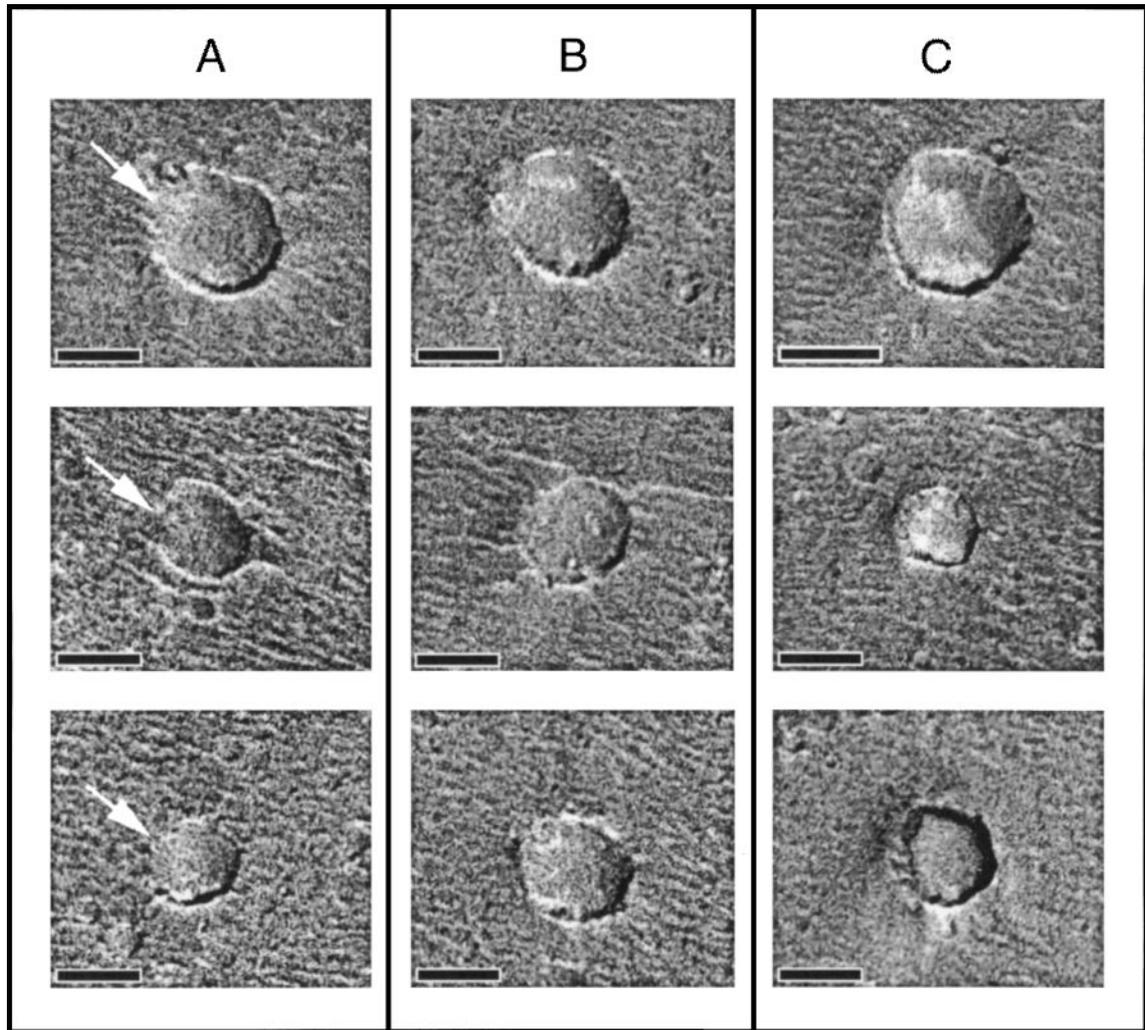
**FIG. 3.** Impact craters near the MPF site showing degradation states of their northwest rims (white arrows): (A) highly degraded west-northwest rims, (B) slightly modified rims, and (C) mostly unmodified rims. Scale bar is 200 m (from MOC images 25603 and 21803). North is toward the top.

with the current wind regime. For example, bright patches of inferred aeolian sediments in craters are found predominantly on the southwest part of the crater floor, consistent with the current direction of the strongest wind. Greeley *et al.* (2000) suggested that the patches could be sheets of fine windblown sediments, or they could be organized into bedforms such as ripples and small dunes, which are smaller than the resolution of the images. These interpretations were confirmed by higher resolution MOC images (Fig. 4) which show that some intra-crater bright material overlaps the crater rims and form bright streaks oriented similar to the bright crater streaks seen on Viking Orbiter images. These features demonstrate that the downwind parts of crater rims are more subject to aeolian resurfacing than other parts of the rim.

The main argument against the interpretation of wind-related modification of the crater rims is the effect of illumination geometry and image resolution (Golombek and Bridges, 2000).

However, if illumination were decisive, then all of the craters should show the same effect. On the contrary, the degraded rims are seen only on the older craters The rim crest appearance depends on illumination direction, with the rims transverse to illumination being more visible than the parts parallel to illumination.

Another example of the illumination effect is seen in the bright ridges in the MPF area (Fig. 4). When the ridges are illuminated parallel to their axes (image SPO-1-25603) they are diffuse, but they appear very sharp under transverse illumination (image M11-2414). Consequently, if some part of the crater rim is highly degraded, the rim crest will be less distinct under all illumination conditions. Imaging of the MPF site by MOC under higher resolution and other illumination directions than earlier images do not show changes in the appearance of the modified craters. Rather, MOC shows more details of the crater interiors (e.g., dune forms) and more distinct bright streaks in the lee of the
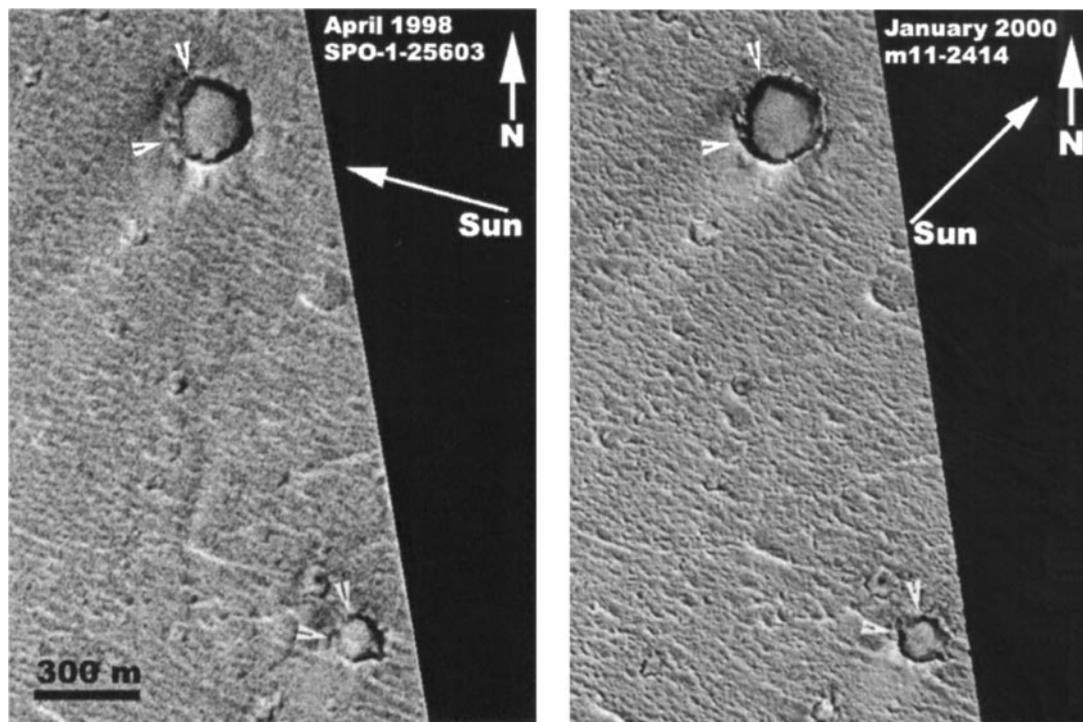
**FIG. 4.** Comparison of the MPF area viewed in April 1998 and January 2000, under different illumination conditions and resolutions. The crater rim crests and both the intra- and inter-crater transverse dunes appear sharp when the illumination is oriented perpendicular to their axes (right side; MOC 2-197, resolution 1.5 m/pixel); conversely they appear more diffuse when the illumination is parallel to their axes (left side; MOC 25603, resolution 3.23 m/pixel). The short white arrows show the modified rim crests (seen on both images) in the west-northwest sector of the craters.

craters. Moreover, comparison of MOC images (SPO-1-25603 and M11-2414; Fig. 4) taken under different illumination shows that some segments of the west-northwest rims of relatively young craters are more degraded.

In addition to the analysis of craters <300 m in diameter, we also mapped the morphology of Big Crater (~1.33 km in diameter) using the stereo MOC images (Fig. 5). Results show some wind modification patterns of its rim similar to those of the smaller craters, including both wind deposition and erosion on the west-northwest and east-southeast parts of the crater rims. As seen in Fig. 5, the rim of Big Crater is notably asymmetric, being narrower and smoother in the west-northwest part than in the east-southeast part. The intra-crater dunes have orientations perpendicular to the orientations of the transverse dunes outside Big Crater, inferred to represent the current wind regime (Greeley *et al.* 2000). Aeolian deposits cover the west-northwest
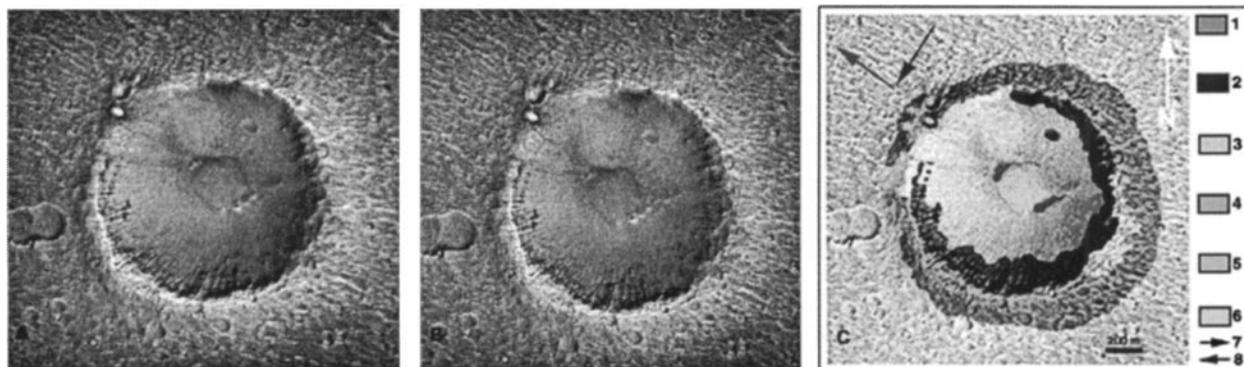


**FIG. 5.** Stereo MOC images (a: MOC 2703, resolution 2.55 m/pixel; b: MOC 25603, resolution 3.23 m/pixel) and a geomorphic map of Big Crater (MPF site). Legend: 1,2—crater rim; 3—rim, modified by wind erosion; 4—depressions on the west-northwest rim slope, interpreted to form by wind deflation; 5—intra-crater aeolian mantle deposits; 6—transverse dunes field; 7—modern wind direction; 8—paleowind direction. North is toward the top.
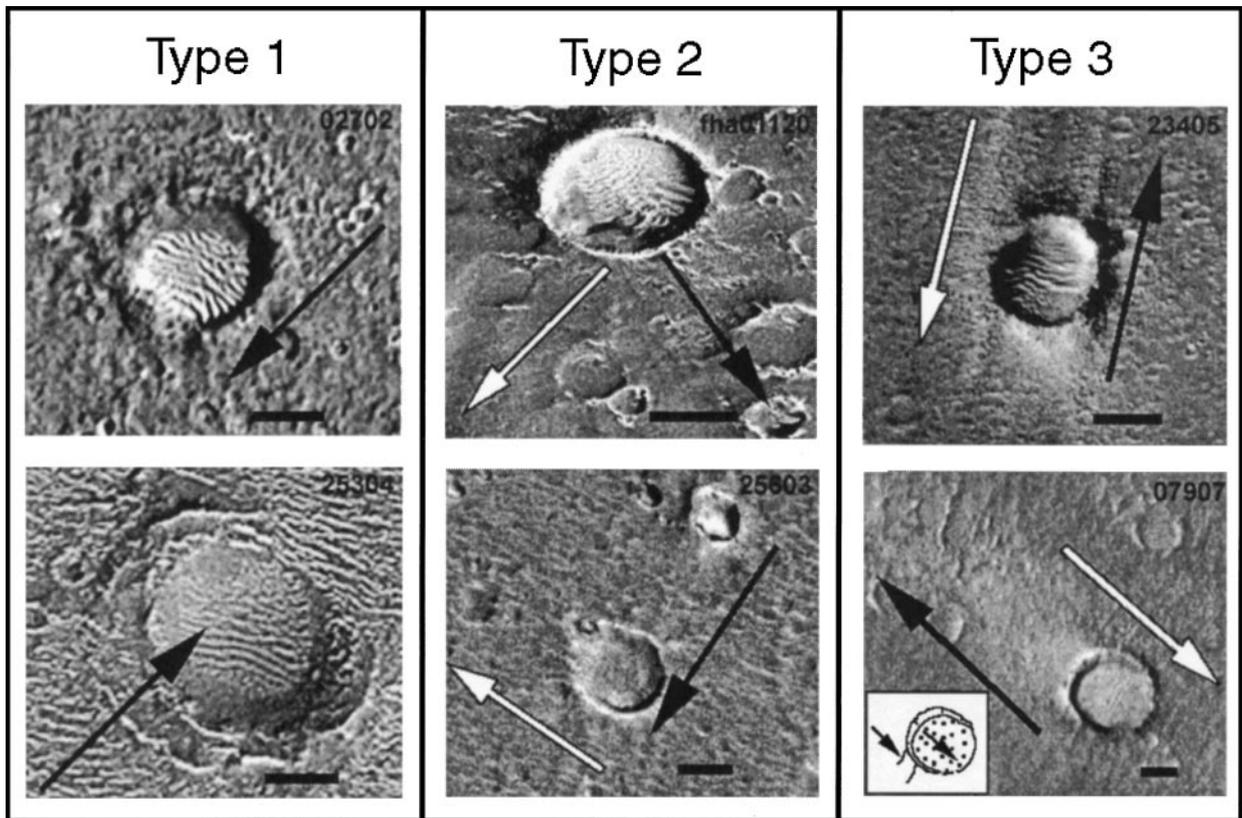
**FIG. 6.** Morphological types of the wind-related modification of the impact craters. Arrows show wind directions. Scale bar is equal to 200 m. Type I involve unidirectional wind, Type 2 involves two orthogonal winds, and Type 3 involves two winds in opposite directions. Parts of the MOC image: 02702 and 25304 (Type 1), 01120 and 25603 (Type 2), and 23405 and 07907 (Type 3).

part of the crater interior slope and mantle the layered and radially ridged structure of the interior crater walls, seen in other parts of the crater. The exterior slope in the west-northwest flank of the crater rim is complicated by shallow linear depressions, which might reflect deflation downwind from the crater rim. The east-southeast rim shows less evidence of wind erosion and is represented only by shallow grooves cutting the rim crest. Thus, the observed morphological patterns associated with wind modification of Big Crater rim and its interior support the suggestion that the crater was subjected to winds from the southeast, similar to the smaller impact craters in the MPF area.

### 2.2. Wind-related Modification of the Impact Craters in Other Regions of Mars

To compare aeolian resurfacing of the craters in other parts of Mars with features at the MPF site, we analyzed craters ∼0.3 to 1 km in diameter in Isidis, Utopia and Elysium Planitiae, and Nirgal Valles (Fig. 1). MOC images show a wide variety of aeolian features within the craters, including intra-crater wind deposits and rim degradation patterns (Kuzmin and Greeley 2000). The features also include drifts and mantles, transverse duneforms inside and near the craters, and bright or dark wind streaks associated with the craters. Erosion features include saddles, nick-like forms, and grooves cut into the rims. In many cases, the inferred wind modification led to asymmetry of the crater rims, in which the upwind parts are usually less degraded than the downwind part (Fig. 6) which is narrower, lower, or even absent. In many cases, the outer crater rim flank is striated. In other cases, the downwind rims are eroded completely, allowing passage of transverse dunes from the interior of the crater.

Analysis of MOC images suggests three main types of winds modified craters (Fig. 6). Type I craters have intra-crater deposits, such as drifts and transverse dunes,which are oriented perpendicular to the wind in the downwind part of the craters and which cover the interior slope. The downwind rim is notably degraded and smoothed, or removed completely (Fig. 6, Type I). These craters are inferred to represent a dominant unidirectional wind regime. Type 2 craters show two orientations of intra-crater duneforms and a wider sector of the rim being degraded. Moreover, the orientations of the duneforms around the craters are inconsistent with the location of the degraded part of the crater rims and the orientations of the intra-crater transverse dunes. These craters appear to be subjected to two prevailing winds, typically orthogonal to each other. These could reflect seasonal and/or paleowind regimes. In Type 3 craters, there is

less degradation, and two dominant, opposite wind directions are involved. These craters, which are rare, include levee-like features in the wind "shadow" of the crater for two inferred wind regimes. These features could represent sand deposits, which shift from one side to the other with alternating winds. In other cases, such as in Nirgal Vallis, evidence for two opposite wind directions include bright diffuse wind streaks and parallel ridges inferred to be transverse dunes. The contact of the ridges with the crater rims suggests that the ridges are formed by winds which are reversed to (i.e., from the northwest) those of the bright streaks. In addition some of the intracraters deposits lap over the souteast rims, consistent with winds from the northwest.

These examples of wind-related modifications of impact craters suggest that the morphological patterns of the crater rim degradation and the associated aeolian features might serve as reliable indicators of the both modern and past wind dynamics and regime. However, it is important to understand the relationships among crater morphology, wind regime, and overall topography. To gain this understanding, topographically forced circulation patterns and atmosphere-surface interactions for flow over small impact craters were studied, based on the results of numerical models.

## 3. MARS REGIONAL ATMOSPHERIC MODELING SIMULATION (MRAMS)

MRAMS is a nonhydrostatic mesoscale model that has been adapted to Mars (Rafkin *et al.* 2001) from a terrestrial version designed to simulate regional and local atmospheric circulation (Pielke *et al.* 1992). The radiation parameterization is identical to that used in the NASA Ames General Circulation Model (Pollack *et al.* 1990). In this study the MRAMS was used to investigate the complex nature of topographically forced circulation patterns and atmosphere–surface interactions for flow over small impact craters.

### 3.1. Initialization and Configuration of the Model

The model atmosphere is initialized in the following manner. A horizontally homogeneous temperature profile with a uniform stability of $1.0 \times 10^{-4}\,\text{s}^{-1}$ is used to initialize a two-dimensional simulation over a flat surface. The model is then run for two sols beginning and ending slightly before sunrise. The location of the domain is that of the MPF landing site corresponding to $\sim L_s = 142°$. After two sols, the simulated atmosphere produces a representative boundary layer profile and exhibits the expected diurnal variation by the start of the second sol. The atmospheric profile from the two-dimensional simulation is used to initialize the three-dimensional crater simulation (Fig. 7). The initial wind profile is a uniform westerly wind of 10 m/s at all levels.

The surface topography for the crater was constructed from a two-dimensional profile of a 3.67-km crater obtained from the MOLA (Garvin and Frawley 1998). This profile was scaled to a 1-km crater diameter to simulate Big Crater (Fig. 8).
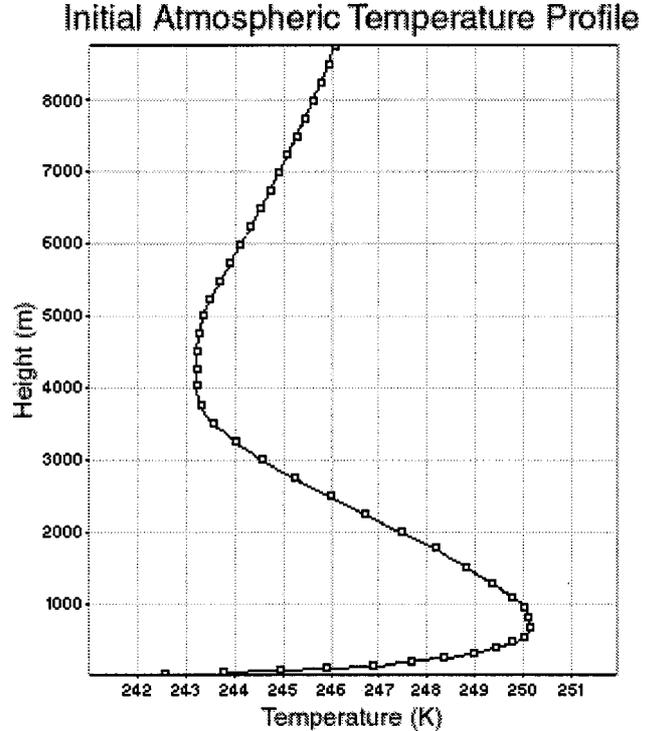


**FIG. 7.** Atmospheric temperature profile used to initialize the three-dimensional crater simulation. A strong nocturnal inversion is present below $\sim$800 m.

The model domain is covered by two (two-way nested) computational grids. The first grid is 40 by 40 points in the horizontal with a grid spacing of 500 m and 47 points in the vertical with the lowest level at 12 m above the surface. The vertical grid spacing is gradually stretched with height to a maximum spacing of 250 m. The total height of the domain is approximately 9 km. The vertical model levels are terrain-influenced and follow the contours of the surface near the surface and gradually flatten with height. The second grid is 102 by 67 points in the horizontal with a grid spacing of 100 m. The vertical grid spacing of the second grid is the same as the first. The second grid is centered on the crater and nested within the coarser first grid. The higher resolution of the second grid allows the computational power to be focused where it is most needed.

### 3.2. Results of the Simulations

MRAMS predicted the wind friction velocities and the flow field around a crater stylized for Big Crater during a 12-hour daily period from sunrise for a mean westerly wind of 10 m/s. Prior to the development of a highly unstable convective boundary layer (over the few hours after sunrise), the wind flow is nearly laminar around the crater. The highly stable nocturnal inversion requires most of the impinging air to flow around the topographic obstacle. Surface friction reduces the low-level wind speeds. The crater rims are subjected to speeds higher than the surrounding surfaces. The friction velocity increases with wind
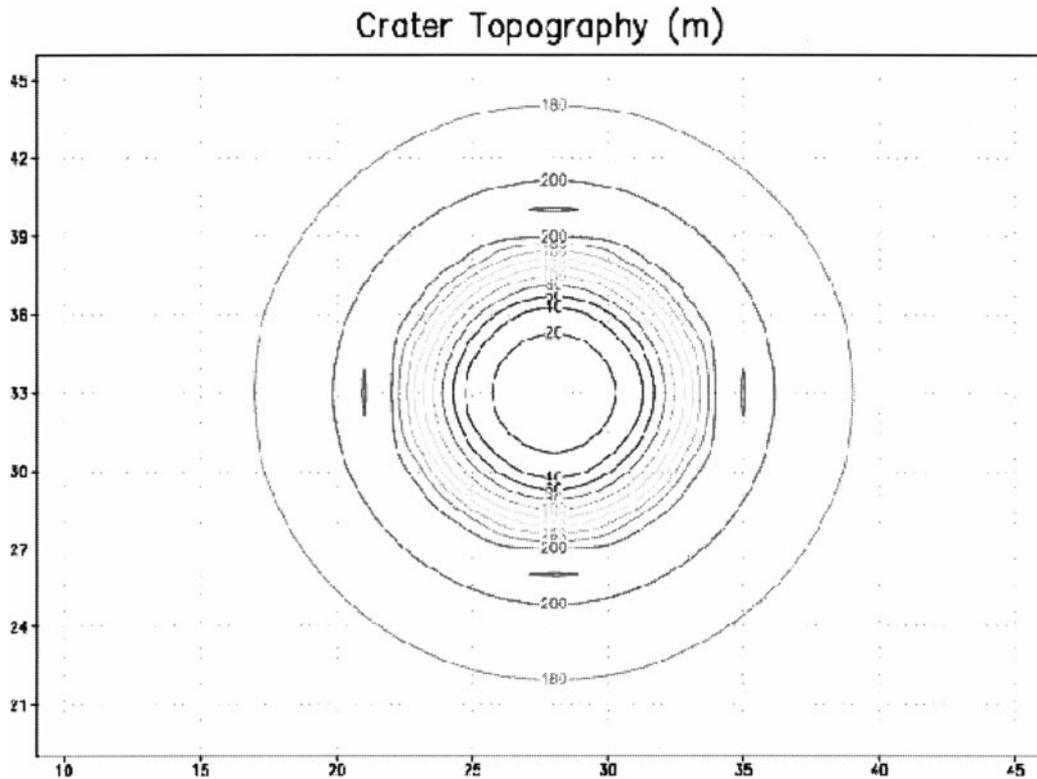
**FIG. 8.** Contour map used for the simulation of wind flow over a small crater. The crater floor is ~150 m below the surrounding area and the crater rim is ~30 m (derived from MOLA data).

speed and exerts a greater stress on particles exposed at the surface, leading to their removal. As seen in Figs. 9a and 9b, the values of the friction velocity are notably higher within the upwind and downwind parts of the rim than outside and inside the crater, but the greatest values of surface stress are on the downwind part of the crater rim. It is notable that the highest values of the friction velocity are organized in bands along the downwind rim perpendicular to the mean flow. These bands are associated with eddy circulation gusts originating within this part of the crater. A broad region of higher surface stress is also found in the lee of the crater, consistent with previous studies (Greeley *et al.* 1974). The maximum predicted friction velocities are ~0.5 m/s with a 5-cm aerodynamic roughness length and 10 m/s free stream wind velocity.

A few hours after sunrise, the depth of the unstable convective boundary layer grows to several kilometers and the atmosphere within this layer becomes highly trubulent. The adiabatic and superadiabatic atmosphere "feels" no downward directed buoyancy-driven restoring force, and the air is free to flow over rather than around the crater. Superposed on the crater circulation are boundary layer convective "rolls" aligned parallel to the mean atmospheric shear vector. The juxtaposition of the crater and convective circulation produces a nonsteady turbulent region in the lee of the crater, which sweeps out a wedge-shaped area in the lee of the crater (Figs. 9c and 9d). The maximum values of the surface shear stress gradually increase to values

slightly in excess of 1.0 m/s. Maximum values are again found on the downwind rim of the crater and occasionally in the turbulent region downwind of the crater. The leeward rim experiences moderate to high stress values that are typically less than those on the downwind rim.

The simulation was terminated ~12 hours into the numerical integration. Future modeling will examine the atmosphere-surface interaction as the sun sets and the nocturnal inversion redevelops.

## 4. DISCUSSION AND CONCLUSIONS

The evidence for wind-related modification of the downwind sector of the craters and other aeolian features near the MPF site serves as morphologic indicators for current and paleowind regimes. Analysis of MOC images for other several regions of Mars shows similar morphological patterns of wind-related modification of small craters. In the regions containing wind-blown materials, craters 0.3 to 1 km in diameter appear to be optimal for assessing regional wind regimes on Mars. Smaller craters are probably subject to rapid burial, while larger craters might require longer times for aeolian features to develop, and for the pristine crater shape to be modified. The rates of crater modification by the wind probably depend on crater exposure age, the dominant wind regime, the flux of windblown particles, and on physical properties of the surface materials where the craters
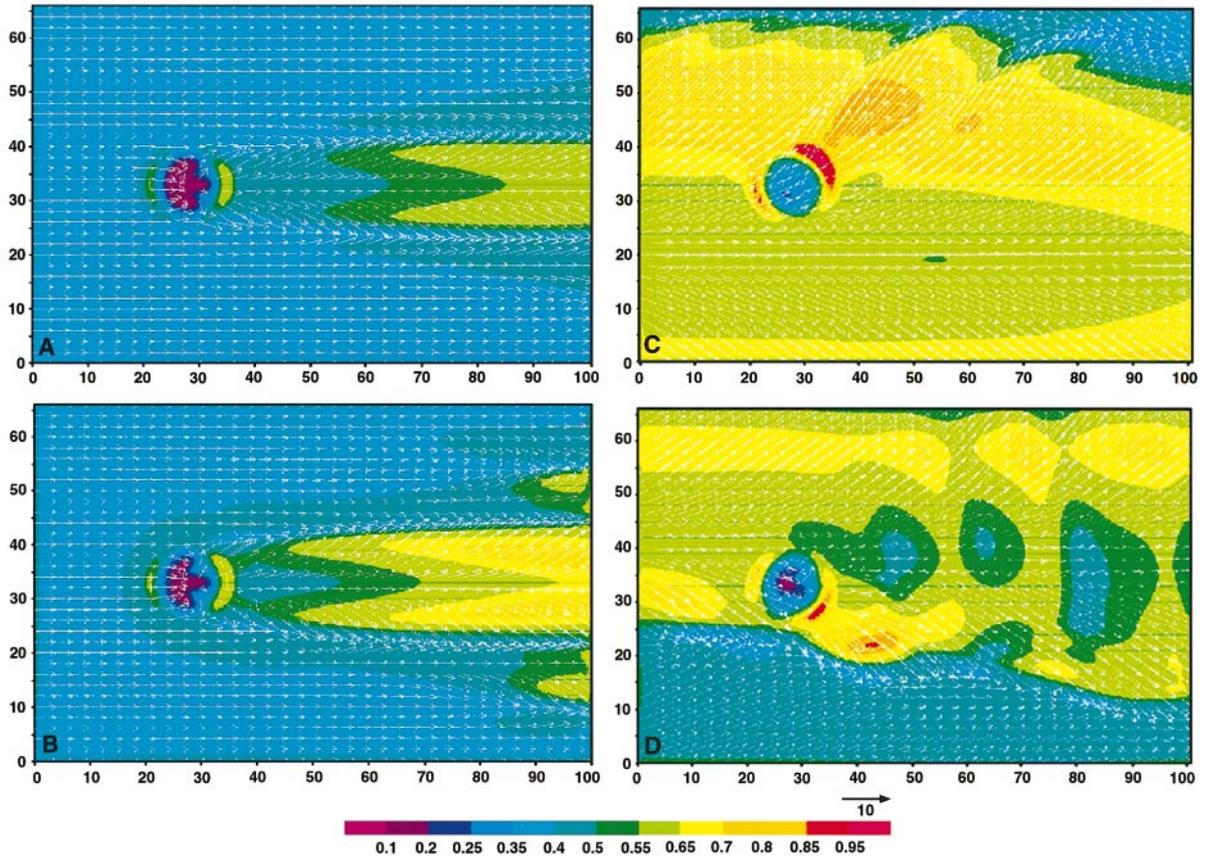
**FIG. 9.** Model predictions of the surface friction velocity (in m/s, colored) and wind vectors (white arrows) around a crater stylized on Big Crater at the MPF site. A,B—for the first 4–5 hours prior to development of deep and convectively unstable boundary layer. Maximum friction velocities are found on the downwind crater rim and in the lee of the crater. Moderate to high friction velocities are also found on the windward rim; C,D—a period when the boundary layer is convectively unstable. Panels C and D are one hour apart. The higher friction velocity found east-west to the north of the crater is a signature of boundary layer convection. The superposition of the crater circulation produces locally higher values on the downwind crater rim, in the lee of the crater. In panel D, the turbulent region in the rear of the crater has shifted from a southwest-to-northeast orientation to a northwest-to-southeast orientation. The east-west running friction velocity signatures of the boundary layer convection are still evident. Wind vectors are scaled according to the 10 m/s arrow shown above the right-hand side of the friction velocity scale.

were formed. If the small craters formed in unconsolidated sediments, such as fluvial or aeolian deposits, then their morphology might be altered significantly by wind erosion and deposition in a shorter time than craters formed in more coherent target materials. Most of the craters in the MPF site formed in fluvial and aeolian deposits (Golombek *et al.* 1997, Ward *et al.* 1999, Greeley *et al.* 1999), which are probably unconsolidated. Under the current strongest winds (from NE to SW), none of the wind erosion patterns are observed on the downwind part of the crater rims. Only intra-crater dunes patches and wind streaks in the lee of the relatively younger craters correlate with these winds. We suggest that the erosion seen on the northwestern parts of the crater's rim could represent paleowinds which were stronger than current winds. A recent study of the influence of obliquity variations on the Martian climate (Haberle, Murphy, and Schaeffer, 2001) shows that the wind surface stress might frequently exceed particle threshold. Under such conditions, there would be an increase in saltation flux and inten-

sify erosion and deflation, leading to degradation of crater rims. Along with wind erosion, aeolian processes might include redistribution intra-crater material across the rim to lee sides of the craters.

MOC images show many areas on Mars which have been mantled and exhumed by aeolian processes (Edgett and Malin 2000). The absence of distinctive patterns of the ejecta around small and relatively young craters in the MPF site (including Big Crater) suggests that the surface has undergone sediment accumulation aggradation, rather than exhumation processes. However, the crater interiors could be partly filled by aeolian deposits which later were subjected to some deflation. Even if the areas around the craters were subjected to exhumation, the terrain would still reflect strong winds from a dominant direction.

The Mars Regional Atmospheric Modeling Simulation shows that maximum values of wind surface stress occur on the downwind rim of small craters and in the turbulent region downwind

**TABLE I**
**The Diameters and the Trends of the Eroded Part of the Crater Rims around MPF Landing Site**

| NN | Diameter (m) | Trends (deg) | NN | Diameter (m) | Trends (deg) |
|---|---|---|---|---|---|
| 1 | 59.4 | 317.5 | 41 | 112.2 | 288.5 |
| 2 | 72.6 | 294 | 42 | 112.2 | 299 |
| 3 | 72.6 | 290 | 43 | 118.2 | 293 |
| 4 | 72.6 | 286 | 44 | 118.8 | 287 |
| 5 | 72.6 | 298.5 | 45 | 118.8 | 295.5 |
| 6 | 72.6 | 276 | 46 | 118.8 | 289 |
| 7 | 72.6 | 311 | 47 | 118.8 | 288 |
| 8 | 79.2 | 293 | 48 | 118.8 | 253 |
| 9 | 79.2 | 293.5 | 49 | 125.4 | 288 |
| 10 | 79.2 | 295.5 | 50 | 125.4 | 293 |
| 11 | 85.8 | 309 | 51 | 125.4 | 281.5 |
| 12 | 85.8 | 288 | 52 | 125.4 | 308 |
| 13 | 85.8 | 293.5 | 53 | 125.4 | 290 |
| 14 | 92 | 312 | 54 | 125.4 | 296.5 |
| 15 | 92.4 | 287 | 55 | 132 | 297 |
| 16 | 92.4 | 306 | 56 | 132 | 253 |
| 17 | 92.4 | 285.5 | 57 | 132 | 290 |
| 18 | 92.4 | 302 | 58 | 132 | 296 |
| 19 | 92.4 | 294 | 59 | 138.6 | 311 |
| 20 | 92.4 | 297 | 60 | 138.6 | 290.5 |
| 21 | 99 | 287 | 61 | 138.6 | 298 |
| 22 | 99 | 292.5 | 62 | 138.6 | 293 |
| 23 | 99 | 289 | 63 | 138.6 | 304 |
| 24 | 99 | 292.5 | 64 | 145.2 | 304 |
| 25 | 99 | 292 | 65 | 145.2 | 300 |
| 26 | 99 | 287 | 66 | 145.2 | 301.5 |
| 27 | 99 | 291 | 67 | 145.2 | 292 |
| 28 | 99 | 290 | 68 | 145.2 | 289.5 |
| 29 | 99 | 285.5 | 69 | 158.4 | 290 |
| 30 | 105.6 | 302 | 70 | 158.4 | 287.5 |
| 31 | 105.6 | 290 | 71 | 158.4 | 291 |
| 32 | 105.6 | 286 | 72 | 158.4 | 308 |
| 33 | 105.6 | 288 | 73 | 171.6 | 270 |
| 34 | 105.6 | 295.5 | 74 | 204.6 | 286 |
| 35 | 105.6 | 290 | 75 | 211.2 | 288 |
| 36 | 112.2 | 305 | 76 | 224.4 | 283.5 |
| 37 | 112.2 | 293 | 77 | 231 | 290.5 |
| 38 | 112.2 | 298 | 78 | 250.8 | 270 |
| 39 | 112.2 | 313.5 | 79 | 270.6 | 291.5 |
| 40 | 112.2 | 291.5 | | | Average: 294.289474 |
| | | | | | maximum: 317.5 |
| | | | | | minimum: 276 |

eccentricity. These parameters vary significantly on time scales of $10^5$ to $10^6$ years (Ward, 1979, Bills, 1990). On longer time scales, they vary chaotically with obliquity excursions as high as 60° (Laskar and Robutel 1993, Touma and Wisdom 1993). However, general circulation model (GCM) simulations with the Geophysical Fluid Dynamics Laboratory (GFDL) model do not show much change in wind direction at the Pathfinder site for different obliquities (Fenton and Richardson 2000). Similar results have been obtained with the NASA/Ames GCM (Haberle *et al.* in preparation), as shown in Fig. 10.

The reason obliquity changes do not have much effect on global wind directions in the MPF area is that they do not fundamentally alter the nature of the Hadley circulation. The near surface flow will always be directed toward the north or the south, and the resultant Coriolis effect will deflect the flow such that the winds will blow from the southwest or the northeast, but never from the southeast (Fig. 10). Thus, while the intensity and latitudinal extent of the Hadley circulation does change when orbit parameters change, the basic wind directions do not. Changes in eccentricity and argument of perihelion also cannot alter the fundamental nature of the Hadley circulation.
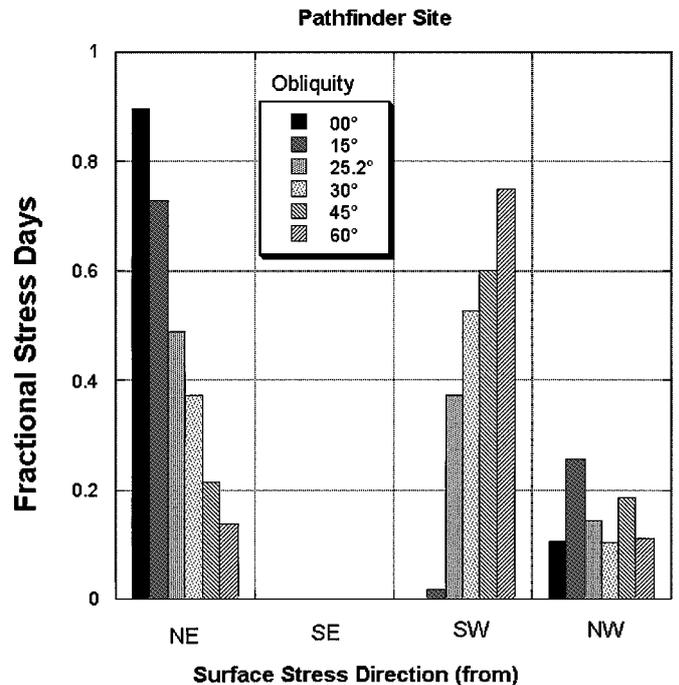


**FIG. 10.** Histogram showing the daily distribution of wind directions at the Pathfinder site for six different obliquity simulations based on the NASA/Ames Mars General Circulation Model (Haberle *et al.* 2000). Fractional stress days are defined to be the daily averaged stress direction (binned into the four cardinal quadrants) weighted by its magnitude, integrated over the year, and normalized by the annually integrated stress. NE refers to a stress vector oriented from the northeast toward the southwest. A similar definition applies to southeast (SE), southwest (SW), and northwest (NW). As is evident, the prevailing wind directions for all obliquities are either from the northeast or from the southwest. In none of these simulations do southeasterly stresses occur.

from the crater, becoming stronger with increasing wind speeds. This pattern is consistent with observations of wind-related modifications of the craters at the MPF site and in other regions of Mars.

If the southeasterly winds inferred from the eroded craters at the MPF site are indicative of atmospheric circulation patterns over a larger area, then how do such winds occur? Bridges *et al.* (1999) and Greeley *et al.* (2000) speculated that the ventifacts and eroded crater rims might have formed when Mars' orbit parameters were different than they are today. The orbit parameters which affect the climate system include the obliquity and

We note that the GCM predicts the general trend of wind directions and often does not reproduce regional near surface winds which are strongly influenced by meso-scale topography. It is possible that anomalous weather patterns, local topography, and diurnal patterns could lead to winds in the present environment which could correlate with the inferred paleowind regime. For example, nighttime heating contrasts between the topographically lower and darker surface of Chryse Planitia with the surrounding higher albedo highlands could generate strong winds. This contrast could lead to even stronger winds during high obliquity periods.

Alternatively, the inferred winds from the southeast could have been produced by large-scale circulation at a time in the past when the planet's spin pole was in a different geographic location than at present Schultz and Lutz (1988) have invoked such a shift—known as "polar wander"—to explain the layered deposits and other features observed in the equatorial region, such as the layered deposits of Medussae Formation and in Arabia Terra. To produce the inferred southeasterlies at the MPF site, the northern pole would have been approximately at $320°$ W in southern Arabia Terra. To produce the inferred southeasterlies at the MPF site, the northern pole would have been approximately at $320°$ W in southern Arabian near the crater Janssen.

To distinguish among these possibilities, further global analysis must be conducted of potential ancient wind-related features in different regions of the planet. If further mapping reveals a more random distribution of inferred ancient wind directions around the planet, then this would argue in favor of local meteorological control. But if the southeasterlies inferred near the MPF site extend throughout most latitudes in that longitude sector, then it would imply that they formed by the large-scale circulation. This would lend support to the polar wander hypothesis.

## ACKNOWLEDGMENTS

## REFERENCES

Bills, B. G. 1990. The rigid body obliquity history of Mars. *J. Geophys. Res.* **95**, 14,137–14,153.

Bridges, N. T., R. Greeley, A. F. C. Haldemann, K. E. Herkenkenhoff, M. Kraft, T. J. Parker, and A. W. Ward 1999. Ventifacts at the Pathfinder landing site. *J. Geophys. Res.* **104**, 8595–8615.

Edgett, K. S., and M. C. Malin 2000. New views of Mars eolian activity, materials, and surface properties: Three vignettes from the Mars Global Surveyor Mars Orbiter Camera. *J. Geophys. Res.* **105**, 1623–1650.

Fenton, L. K., and M. I. Richardson 2000. Global sand transport as predicted by the GFDL Mars GCM. *Lunar Planet Sci.* **31**, 2072 (abstract), Lunar and Planetary Institute, Houston (CD-ROM).

Garvin, J. B., and J. J. Frawley 1998. Geometric properties of martian impact craters: Preliminary results from the Mars Orbiter Laser Altimeter. *J. Geophys. Lett.* **25**, 4405–4408.

Golombek, M. P. and 14 colleagues 1997. Overview of the Mars Pathfinder mission and assessment of landing site predictions. *Science* **278**, 1743–1748.

Golombek, M. P., and N. T. Bridges 2000. Erosion rates on Mars and implication for climate change: Constraints from the Pathfinder landing site. *J. Geophys. Res.* **105**, 1841–1853.

Greeley, R., J. D. Iversen, J. B. Pollack, N. Udovich, and B. R. White 1974. Wind tunnel simulations of light and dark streaks on Mars. *Science* **183**, 847–849.

Greeley, R., M. Kraft, R. Sullivan, G. Wilson, N. T. Bridges, K. Herkenhoff, R. O. Kuzmin, M. Malin, and W. Ward 1999. Aeolian features and processes at the Mars Pathfinder landing site. *J. Geophys. Res.* **104**, 8578–8584.

Greeley, R., M. Kraft, R. O. Kuzmin, and N. T. Bridges 2000. Mars Pathfinder landing site: Evidence for a change in wind regime from lander and orbiter data. *J. Geophys. Res.* **105**, 1829–1840.

Kuzmin, R. O., and R. Greeley 1999. Local and regional aeolian geomorphology at the Mars Pathfinder landing site area: Evidence for paleowind regime. *Lunar Planet. Sci.* **30**, 1415 (abstract), Lunar and Planetary Institute, Houston (CD-ROM).

Kuzmin, R. O. and R. Greeley 2000. Wind-related modification of the meteorite crater morphology as key to wind regime history on Mars. *Lunar Planet. Sci.* **31**, 1643 (abstract), Lunar and Planetary Institute, Houston (CD-ROM).

Laskar, J., and P. Robutel 1993. The Chaotic obliquity of the planets. *Nature* **361**, 608–612.

Pielke, R. A., and W. R. Cotton, R. L. Walko, C. J. Tremback, W. A. Lyons, L. D. Grasso, M. E. Nicholls, M. D. Moran, D. A. Wesley, T. J. Lee, and J. H. Copeland 1992. A comprehensive meteorological modeling system—RAMS. *Meteor. Atmos. Phys.* **49**, 69–91.

Pollack, J. B. D., R. M. Haberle, J. Schaeffer, and H. Lee 1990. Simulations of the general circulation of the martian atmosphere I: Polar Processes. *J. Geophys. Res.* **95**, 1447–1474.

Rafkin S. C. R., R. M. Haberle, and T. I. Michaels 2001. The Mars regional atmospheric modeling system: Model description and selected simulations. *Icarus*, submitted.

Schultz, P. H., and A. B. Lutz 1988. Polar wandering of Mars. *Icarus* **73**, 91–141.

Smith, P. H. and 29 colleagues 1997. Results from the Mars Pathfinder camera. *Science* **278**, 1758–1765.

Touma, J., and J. Wisdom 1993. The chaotic obliquity of Mars. *Science* **259**, 1294–1297.

Ward W. R. 1974. Climatic variations on Mars 1. Astronomical theory of insolation. *J. Geophys. Res.* **79**, 3375–3386.

Ward, A. W., L. R. Gaddis, R. L. Kirk, L. A. Soderblom, K. L. Tanaka, M. P. Golombek, T. J. Parker, R. Greeley, and R. O. Kuzmin 1999. General geology and geomorphology of the Mars Pathfinder landing site. *J. Geophys. Res.* **104**, 8555–8571.